BASIC RESEARCH

Nanomedicine: Nanotechnology, Biology, and Medicine
12 (2016) 377–386

nanomedicine
Nanotechnology, Biology, and Medicine

ELSEVIER

Original Article

nanomedjournal.com

Stable loading and delivery of disulfiram with mPEG-PLGA/PCL mixed nanoparticles for tumor therapy

Wantong Song, PhD[a], Zhaohui Tang, PhD[a,*], Tian Lei, BPharm[b], Xue Wen, BSc[c], Guanyi Wang, BSc[a], Dawei Zhang, BPharm[a], Mingxiao Deng, PhD[c], Xing Tang, PhD[b,*], Xuesi Chen, PhD[a,*]

[a]*Key Laboratory of Polymer Ecomaterials, Changchun Institute of Applied Chemistry, Chinese Academy of Sciences, Changchun, PR China*
[b]*School of Pharmacy, Shenyang Pharmaceutical University, Shenyang, PR China*
[c]*Department of Chemistry, Northeast Normal University, Changchun, PR China*

Received 22 August 2015; accepted 10 October 2015

Abstract

Disulfiram (DSF) showed great potential in an *in vitro* tumor therapy study; however, those results could not be applied to an *in vivo* study due to the extreme instability of DSF in blood. Here, we describe a system of methoxy poly(ethylene glycol)-*b*-poly(lactide-*co*-glycolide)/poly(ε-caprolactone) (mPEG-PLGA/PCL) mixed nanoparticles (NPs) for DSF loading and delivery. By adjusting the mPEG-PLGA/PCL content ratios, the DSF loading capacity increased to 7.8%, while the hydrodynamic radii of the NPs were around 50-100 nm. The DSF-loaded NPs showed high stability in distilled water and 10% serum-containing phosphate buffered saline. The NPs efficiently protected DSF from degradation while maintaining its anti-tumor properties. Furthermore, a pharmacokinetics study demonstrated that NP delivery system enhanced the DSF concentration in the blood after tail vein injection. Finally, DSF delivery using this model effectively slowed the growth of a 4T1 murine xenograft tumor.

From the Clinical Editor: The anti-tumor efficacy of the anti-alcoholic drug disulfiram has been known for some time. However, its use in the clinical setting is limited due to the underlying instability of the drug. In this study, the authors utilized a nanocarrier system of mPEG-PLGA/PCL for the delivery of this drug. The promising results may allow encapsulation of other drugs.

Key words: Disulfiram; Drug delivery; Nanoparticles; mPEG-PLGA; PCL

The costs of bringing new drugs to market are exceedingly high; therefore, the repurposing of existing drugs for new uses has become a shortcut for drug development.[1,2] Disulfiram (tetraethylthiuram disulfide, DSF) is a member of the dithiocarbamate family that has been categorized as a "repurposed drug".[3] DSF has traditionally been used for decades in the treatment of alcoholism due to its ability to irreversibly inhibit the acetaldehyde dehydrogenase (ALDH).[4] In recent years, researchers have discovered that DSF and its metabolites may have antitumor and chemosensitizing activities, possibly through inhibition of proteasome activity.[5–8] In fact, high-throughput screening has identified DSF as a potential therapeutic for triple-negative breast cancer cells, breast cancer stem cells and human glioblastoma stem cells by modulating ROS-MAPK and NFκB pathways.[9–12] DSF also permanently inactivates the human multidrug resistance p-glycoprotein and has been approved for prevention of related cases of drug resistance.[13,14] Additionally, the safety of DSF has been fully proven — making it an attractive option for cancer therapy development.

Abbreviations: DSF, disulfiram; mPEG-PLGA, methoxy poly(ethylene glycol)-*b*-poly(lactide-*co*-glycolide); PCL, poly(ε-caprolactone); NPs, nanoparticles; DMF, *N*,*N*′-dimethylformamide; CH_3CN, acetonitrile; DLS, dynamic light scattering; TEM, transmission electron microscopy; CMC, critical micelle concentration; HPLC, high-performance liquid chromatography; DLC%, drug loading content; DLE%, drug loading efficacy; *R*%, recovery ratio; PBS, phosphate buffered saline; FBS, fetal bovine serum; SDS-PAGE, sodium dodecyl sulfate–polyacrylamide gel electrophoresis; AUC, area under curve; MRT, mean residence time; T_{max}, time to reach maximum concentration; C_{max}, maximum concentration; $T_{1/2}z$, terminal half life; TSR%, tumor suppression rate; H&E, hematoxylin and eosin.

The authors declare no conflict of interest.

This work was supported by the National Natural Science Foundation of China (Projects 51173184, 51233004, 51373168, 51390484, 51473029, 81430087 and 51403204), and Jilin province science and technology development program (20130206058GX and 20130521011JH).

*Corresponding author at: Key Laboratory of Polymer Ecomaterials, Changchun Institute of Applied Chemistry, Chinese Academy of Sciences, Changchun, PR China.

E-mail addresses: ztang@ciac.ac.cn (Z. Tang), tangpharm@sina.com (X. Tang), xschen@ciac.ac.cn (X. Chen).

http://dx.doi.org/10.1016/j.nano.2015.10.022
1549-9634/

DSF is given as an oral formulation for the treatment of alcoholism, which was the most direct way to test its efficacy as an anti-cancer therapeutic. However, few successful *in vivo* cases have been reported for the oral administration of DSF in mice, even at extremely high doses.[15,16] Oral DSF as a cancer therapeutic has been tested in several completed and on-going trials (ClinicalTrials.gov Identifier NCT00256230, NCT00742911, NCT01118741), but no positive outcomes have been reported. The poor results following oral administration of DSF are due to its extreme instability under physiological conditions; DSF is quickly degraded in the gastrointestinal system, during the hepatic first-pass effect and in the blood stream.[17,18] As a result, orally administered DSF does not reach tumor tissues at therapeutic concentrations, which is a major limitation for the clinical usage of DSF in cancer treatment.

The development of a carrier system that will maintain stability and enable the appropriate distribution of DSF to the tumor tissues is a key issue for ensuring its proper testing as a cancer therapeutic agent. As such, nanocarriers have shown a lot of potential for antitumor drug delivery.[19–21] Nanocarriers 'trap' small molecule drugs, changing their pharmacokinetics and biodistribution while minimizing system toxicity and increasing drug accumulation in the tumor tissue.[22–25] Of importance to DSF in particular, nanocarriers can protect drugs from interacting with the surrounding environment, which prevents premature degradation of unstable drugs in biological systems.[26,27] Previously, a liposome carrier system was used to encapsulate DSF with high efficiency; however, degradation still occurred because the DSF was not completely isolated from the surrounding medium.[28] In contrast, nanoparticles (NPs) provide a hydrophobic inner core that completely entraps the DSF and is therefore a more suitable medium for DSF loading and delivery. Even so, others and we have found it difficult to encapsulate DSF into amphiphilic NPs.[29–33] To the best of our knowledge, Duan et al[34] is the only laboratory to successfully entrap DSF with over 5% drug loading content by applying a shell-crosslinked micelle system. However, the materials applied were not degradable and the structure was complicated, making the system difficult to apply clinically.

In this study, we applied the most commonly polyesters, mPEG-PLGA and PCL, toward DSF encapsulation. Drug-incorporated NPs are usually prepared by nanoprecipitation methods. During this process, the precipitation index and compatibility of the polymer with the drugs are important for successfully encapsulating the drugs inside the formed NPs.[35–37] To obtain high drug loading capability, a high hydrophobic proportion is commonly necessary.[38] Also, thermodynamic stability of the NPs, as commonly determined by the critical micelle concentration (CMC), is an important parameter for stabilizing the encapsulated drug; NPs with lower CMC and higher thermodynamic stability will remain stable and reduce drug leakage during delivery.[39,40] Based on the above analysis, we prepared a series of NPs for DSF loading by adjusting the weight ratios of mPEG-PLGA and PCL. We evaluated the DSF loading capacity, stability, *in vitro* and *in vivo* therapeutic efficacy of this DSF formulation.

Methods

Materials

Methoxy poly(ethylene glycol)-*b*-poly(lactide-*co*-glycolide) (mPEG-PLGA; M_w: mPEG 5000 Da, PLGA 2000 Da, LA/GA 75/25) and poly(ε-caprolactone) (PCL, M_w: 3400 Da) were a gift from Changchun Sinobiomaterials Co., Ltd., China. DSF was bought from Sigma–Aldrich. All the other reagents and solvents were purchased from Sinopharm Chemical Reagent Co. Ltd. and used as received.

Preparation of DSF-loaded NPs with different mPEG-PLGA/PCL ratios

The DSF loaded NPs were prepared using a nanoprecipitation method. The mPEG-PLGA/PCL (90 mg, weight ratios from 9/0-0/9, named $NP_{9/0/1}$-$NP_{0/9/1}$) and 10 mg DSF were dissolved in 5 mL *N*,*N*′-dimethylformamide/acetonitrile (DMF/CH_3CN, 1/1, v/v), then slowly added to 20 mL deionized water under vigorous stirring. The resulting solution was stirred for another 2 h and transferred into dialysis bags (MWCO 3500 Da) and dialyzed against deionized water for 36 h. The solution was then collected, centrifuged at 8000 rpm for 5 min and filtered through a 0.45 μm membrane, which resulted in the final DSF-incorporated NPs solution.

The sizes of the obtained NPs were determined by dynamic light scattering (DLS) using a Wyatt-QELS instrument with a vertically polarized He-Ne laser (DAWN EOS, Wyatt Technology) at 90° collecting optics. Transmission electron microscopy (TEM) images were taken with a JEOL JEM-1011 transmission electron microscope at an accelerating voltage of 100 kV. Critical micelle concentrations (CMC) of the NPs were estimated by fluorescence spectroscopy using pyrene as the probe, following our previously published method.[41] DSF content was determined using a high-performance liquid chromatography (HPLC) system, consisting of a reverse-phase C-18 column (Symmetry), with a mobile phase of acetonitrile and water (80/20, v/v) pumped at a flow rate of 1.0 mL/min. The drug loading contents (DLC%) and drug loading efficacies (DLE%) were calculated by the following equation:

$$\mathrm{DLC\%} = \frac{\mathrm{DSF\ weight}}{\mathrm{total\ NP\ weight}} \times 100\%$$

$$\mathrm{DLE\%} = \frac{\mathrm{DSF\ content\ in\ NPs}}{\mathrm{theoretical\ DSF\ content\ in\ NPs}} \times 100\%$$

The recovery ratios (*R*%) are defined to estimate the yield of the NPs, calculated by the following equation:

$$R\% = \frac{\mathrm{resulted\ NP\ weight}}{\mathrm{total\ material\ weight\ fed}} \times 100\%$$

Stability of the NPs

The feed ratio of mPEG-PLGA/PCL/DSF was 4/5/1 in mass for the prepared NPs ($NP_{4/5/1}$). The $NP_{4/5/1}$ was placed in a 37 °C shaking incubator with a shaking rate of 100 rpm at a concentration of 1.0 mg/ml in distilled water. At predetermined time points (0 h, 24 h, 48 h, 72 h, 96 h), a 0.5 mL aliquot of the

solution was withdrawn and the NP sizes and intensities were measured by DLS.

The stability of $NP_{4/5/1}$ in phosphate buffered saline (PBS) containing 10% fetal bovine serum (FBS) was measured similar to the description above. Specifically, 0.5 mL of the prepared $NP_{4/5/1}$ solution was diluted with 4.0 mL PBS and 0.5 mL FBS, then kept at a 37 °C shaking incubator with a shaking rate of 100 rpm. At predetermined time intervals (0 h, 6 h, 24 h, 48 h, 72 h), a 0.5 mL aliquot of the solution was withdrawn and the NP sizes and intensities were measured by DLS.

Cargo loading stability

Nile red-incorporated NPs were prepared using a nanoprecipitation method similar to that described above, with 40 mg mPEG-PLGA + 50 mg PCL + 5 mg Nile red applied. Then 5 mL of the prepared NPs-Nile red solution was kept at a 37 °C shaking incubator with a shaking rate of 100 rpm. At predetermined time points (0 h, 6 h, 24 h, 48 h, 72 h), a 0.5 mL aliquot of the solution was withdrawn, and diluted to 2.0 mL for fluorescence measurement. The fluorescent detector (PTi, Photon Technology International, Inc.) was set at an excitation wavelength of 543 nm and the emission intensities from 570 to 720 nm were recorded.

The cargo loading stability in PBS containing 10% FBS was also measured using the Nile red-incorporated NPs. The prepared solution (0.5 mL) was added to 4.0 mL PBS and 0.5 mL FBS, then kept at a 37 °C shaking incubator with a shaking rate of 100 rpm. At predetermined time points (0 h, 6 h, 24 h, 48 h, 72 h), a 0.5 mL aliquot of the solution was withdrawn, and then diluted to 2.0 mL for fluorescence measurement.

Stability of free DSF and $NP_{4/5/1}$

Free DSF, dissolved in DMSO and diluted to 0.01 mg/mL using water, or the prepared $NP_{4/5/1}$ (0.01 mg DSF equivalent/mL water) were kept at a 37 °C shaking incubator with a shaking rate of 100 rpm. At predetermined time points (0 h, 4 h, 24 h, 48 h, 72 h, 96 h), a 0.5 mL aliquot of the solution was withdrawn, freeze-dried, and the DSF content was measured by HPLC. Residual DSF (%) was calculated by comparing to the initial DSF concentration.

The stability of free DSF and $NP_{4/5/1}$ in PBS containing 10% FBS was tested similar to the above description; both the free DSF and $NP_{4/5/1}$ (0.01 mg DSF equivalent/mL PBS containing 10% FBS) were kept at a 37 °C shaking incubator with a shaking rate of 100 rpm. At predetermined time points (0 h, 4 h, 8 h, 24 h, 48 h, 72 h), a 0.5 mL aliquot of the solution was withdrawn and freeze-dried, and the DSF content was measured.

Cell culture

The human breast adenocarcinoma cell line, MCF-7, is maintained by our laboratory. The mouse breast cancer cell line, 4T1, was obtained from Shanghai Bogoo Biotechnology Co., Ltd. All the above cells were cultured in DMEM medium supplemented with 10% FBS, 100 U/mL penicillin and 100 U/mL streptomycin and grown in a 37 °C humidified environment containing 5% CO_2.

MTT assay

The cytotoxicity of DSF and $NP_{4/5/1}$ was determined by MTT assay in the MCF-7 and 4T1 cell lines. Cells were seeded in 96-well plates at a density of 7000-10,000 cells per well. After 24 h, free DSF or $NP_{4/5/1}$ was added at predetermined DSF concentrations, and incubated for another 24 or 48 h. At the end of the treatment, 20 μL MTT solution (5.0 mg/mL) was added into each well. The plates were incubated at 37 °C for another 4 h. After the medium was gently removed, 150 μL of DMSO was added, and the plates were agitated for 5 min to dissolve the formazan dye. The optical density (OD) of each well at 492 nm was measured on a Bio-Rad 680 microplate reader. Cell viability (%) was determined according to the following equation: viability (%) = $(A_{sample}/A_{control}) \times 100\%$, where A_{sample} and $A_{control}$ were the absorbance of the sample wells and control wells, respectively.

Pharmacokinetic study

The Laboratory Animal Center of Shenyang Pharmaceutical University provided Sprague Dawley (SD) rats, weighing between 200 and 220 g. Before experimentation, the rats were fasted for 12 h with free drinking water. Then, six rats were randomly divided into two groups, and free DSF (dissolved in Cremophor EL/ethanol at 5.0 mg/mL and diluted to desired concentrations by distilled water) and $NP_{4/5/1}$ were administered via tail vein (DSF dosage, 8.0 mg/kg). At defined time periods (5 min, 15 min, 30 min, 45 min, 1 h, 2 h, 4 h, 6 h, 8 h, 12 h and 24 h), 0.25 mL of blood was collected from the orbital cavity, heparinized, and centrifuged at 6000 rpm for 5 min to obtain the plasma. The plasma samples were instantly handled by phase extraction method (Waters® OASIS HLB, 1 cc/10 mg), and the DSF concentration was measured by a Waters® XEVO™TQMS ACQUITY UPLC® system.

In vivo anti-tumor efficacy test

Balb/C mice (5-6 weeks of age) were bought from Beijing Huafukang Biological Technology Co. Ltd. All the animal experiments were conducted in accordance with the guidelines of the Laboratory Protocol of Animal Care and Use Committee, Jilin University. A 4T1 xenograft tumor model was prepared by inoculating the right flank of Balb/C mice with 2.0×10^6 4T1 cells. After tumor growth reached about 50 mm^3, the mice were randomly divided into three groups ($n = 6$), receiving saline, free DSF, or $NP_{4/5/1}$ via tail vein on days 1, 3, 5, 8, 10 and 12. The dosage of DSF was 15 mg/kg body weight. Measurements of tumor volume and body weight were used to evaluate the treatment efficacy and safety, respectively. Tumor volume (V_t) and tumor suppression rate (TSR%) were calculated based on the following equation:

$$V_t = a \times b^2/2$$

$$\text{TSR\%} = [(V_c - V_x)/V_c] \times 100\%$$

where a and b are the major and minor axes of the tumors measured by caliper. V_c represents tumor volume of the control group; V_x represents tumor volume of the treatment group.

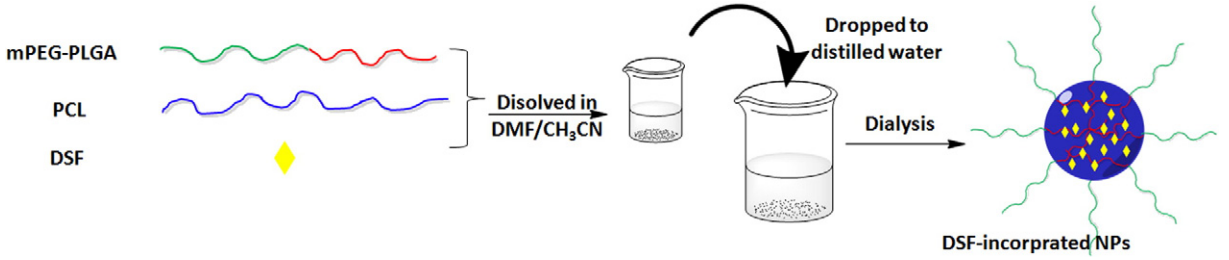

Scheme 1. Preparation of DSF-incorporated mPEG-PLGA/PCL NPs by a nanoprecipitation method.

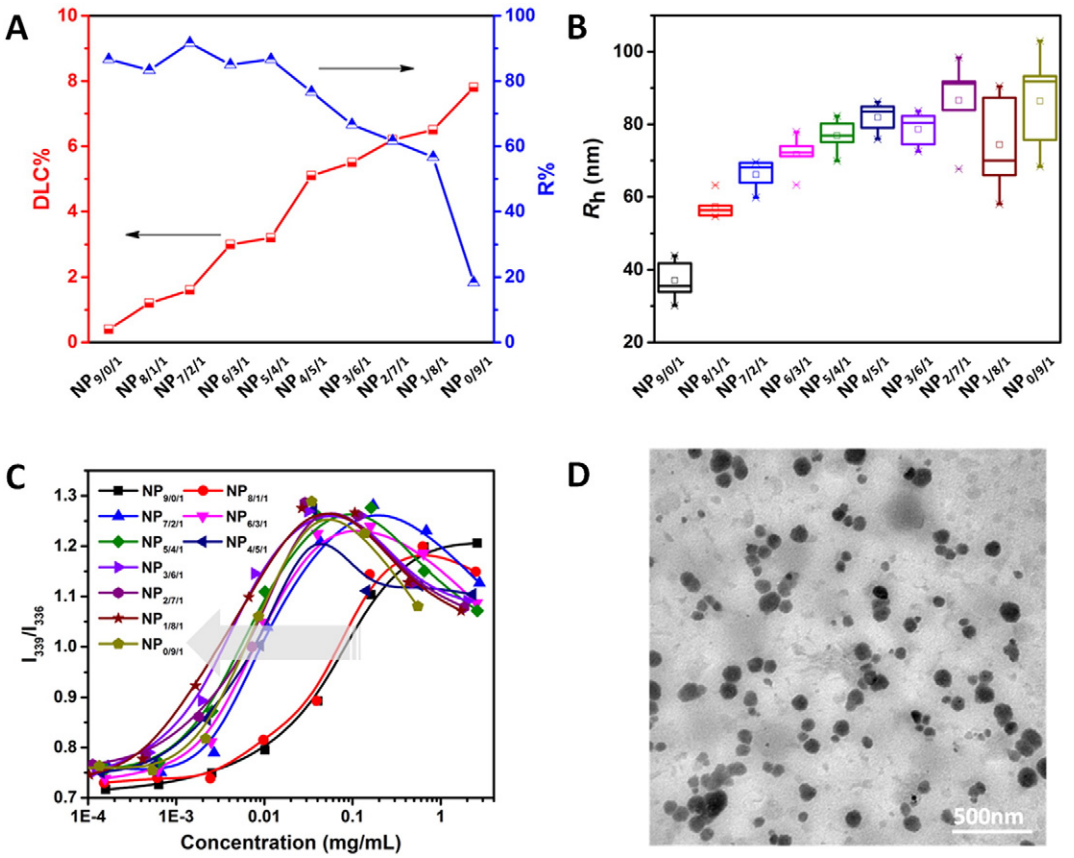

Figure 1. Characterization of the DSF-incorporated mPEG-PLGA/PCL NPs. (**A**) Drug loading content (DLC%) and recycle rate (*R*%). (**B**) Hydrodynamic radius (R_h) of the prepared NPs, measured by DLS. (**C**) I_{339}/I_{336} fluorescent ratios plots concentrations. (**D**) TEM image of $NP_{4/5/1}$.

At the end of the treatment, the mice were sacrificed and the tumors were excised and stained with hematoxylin and eosin (H&E) for histological analysis.

Statistical analysis

All mean values ± SD reported in results section were compared by Student's *t* test. *P* values of <0.05 were considered significant.

Results

Preparation and characterization of $NP_{4/5/1}$

In this study, the nanoprecipitation method shown in Scheme 1 was used to prepare the $NP_{4/5/1}$. We used mPEG-PLGA and PCL with average molecular weights of 5 k-2 k and 3.4 k, respectively. The content ratios of mPEG-PLGA/PCL were changed from 9/0 to 0/9 in order to adjust the properties of the prepared NPs. As summarized in Figure 1, *A* and Table 1, $mPEG_{5k}$-$PLGA_{2k}$ was not a good candidate for DSF loading, resulting in a DLC% of only 0.2% and a DLE% of 2.0% ($NP_{9/0/1}$). The addition of PCL to the system dramatically improved the encapsulation capability of the NPs to DSF, and such an improvement was correlative to the increase of PCL content in the formulation. The encapsulation efficacy was 78% and 65% when the PCL ratios were 90% and 80% ($NP_{0/9/1}$ and $NP_{1/8/1}$). However, an obvious decrease in the recycle ratio (*R*%) of the obtained NPs occurred when the PCL content was over 50% ($NP_{4/5/1}$-$NP_{0/9/1}$), suggesting that when the concentration of PCL is too high, it could not be fully enwrapped inside the mPEG-PLGA shells.

Table 1
Characterization of the prepared NPs.

Entry[a]	Feed/mg			DLC%	DLE%	*R*%	R_h/nm	CMC/10^{-3} mg/mL
	mPEG-PLGA	PCL	DSF					
$NP_{9/0/1}$	90	0	10	0.2	2	86.7	30.1 ± 5.7	19.6
$NP_{8/1/1}$	80	10	10	1.2	12	83.3	54.9 ± 6.2	16.5
$NP_{7/2/1}$	70	20	10	1.6	16	91.7	68.1 ± 7.4	2.78
$NP_{6/3/1}$	60	30	10	3.0	30	85.0	71.2 ± 5.4	1.86
$NP_{5/4/1}$	50	40	10	3.2	32	86.7	76.9 ± 8.7	1.37
$NP_{4/5/1}$	40	50	10	5.1	51	76.7	79.0 ± 9.3	0.85
$NP_{3/6/1}$	30	60	10	5.5	55	66.7	82.3 ± 9.3	0.70
$NP_{2/7/1}$	20	70	10	6.2	62	61.7	91.2 ± 10.5	0.94
$NP_{1/8/1}$	10	80	10	6.5	65	56.7	90.5 ± 12.8	0.71
$NP_{0/9/1}$	0	90	10	7.8	78	18.3	91.8 ± 25.3	1.76

[a] $NP_{x/y/z}$ refers to the feed ratio of mPEG-PLGA, PCL and DSF, with *x*/*y*/*z* being in mass for the preparation of NPs.

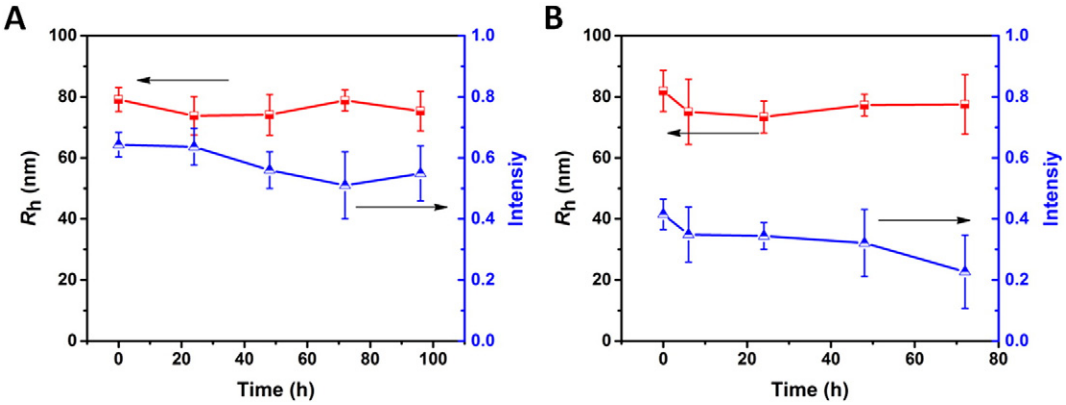

Figure 2. Particle sizes and intensities of $NP_{4/5/1}$ in (**A**) distilled water and (**B**) PBS containing 10% FBS at 37 °C (n = 3).

The hydrodynamic radius (R_h) of the NPs, as measured by DLS, also correlated with the NPs content. As the PCL content increased from 10% to 90%, the R_h increased from 30.1 ± 5.7 nm to 91.2 ± 10.5 nm (Table 1). When the PCL ratios were too high ($NP_{2/7/1}$-$NP_{0/9/1}$), the amount of change in size of the obtained NPs increased (Figure 1, *B*). Additionally, the CMC of the NPs significantly decreased with the addition of PCL (Figure 1, *C*). The CMC of NPs prepared from pure $mPEG_{5k}$-$PLGA_{2k}$ ($NP_{9/0/1}$) was only 19.6×10^{-3} mg/mL; however, when 20% PCL was added, the CMC decreased to 2.78×10^{-3} mg/mL ($NP_{7/2/1}$), and the CMC for $NP_{3/6/1}$ was as low as 0.70×10^{-3} mg/mL (Table 1). CMC is a reflection of the thermodynamic stability of the prepared NPs; a lower CMC suggests that the NPs have a higher thermodynamic stability. This is very important for *in vivo* drug delivery, since a thermodynamically unstable carrier may dissociate before reaching its target and prematurely release the drug.

Based on the above results, in subsequent experiments we used $NP_{4/5/1}$ with DLC% over 5% (5.1%), *R*% over 75% (76.7%), R_h of 79.0 ± 9.3 nm, and CMC of 0.85×10^{-3} mg/mL, with good sphere morphology (Figure 1, *D*).

Stability of $NP_{4/5/1}$

The stability of the $NP_{4/5/1}$ in water was first evaluated by monitoring changes in the size of the NPs. At different time intervals, part of the solution was withdrawn, and the particle sizes and intensities were measured by DLS. As shown in Figure 2, *A*, $NP_{4/5/1}$ was quite stable in distilled water, with no significant size or intensity changes happening within 96 h. Similarly, we measured the stability of the NPs under near-physiological conditions by incubating $NP_{4/5/1}$ in a PBS solution containing 10% FBS at 37 °C. The NP sizes did not change much, although the intensity slightly decreased after 48 h (Figure 2, *B*). These data suggest that PEG 'blocks' are present at the surface of the prepared NPs and prevent non-specific protein adsorption and aggregation on the NPs.[42]

We tested the cargo-loading stability of the NPs by entraping them with Nile red. Nile red is extremely insoluble in water; therefore, if any Nile red molecules diffuse out from the NPs, the fluorescent intensity will decrease.[43] As shown in Figure 3, *A*, the fluorescent intensity of Nile red remained constant during 72 h of observation in water. Similarly, in PBS containing 10% FBS, the fluorescent intensity also remained constant for over 24 h (Figure 3, *B*); a significant decrease in Nile red intensity occurred after 24 h. These results suggest that the mPEG-PLGA/PCL NPs can maintain a stably enwrapped cargo for at least 24 h under physiological conditions.

Since DSF undergoes quick self-catalyzed hydrolysis in water, we could not describe its release profiles.[44,45] Therefore, in order to evaluate the stability of the $NP_{4/5/1}$, we compared the residual DSF concentrations over time. As shown in Figure 4, *A*, free DSF

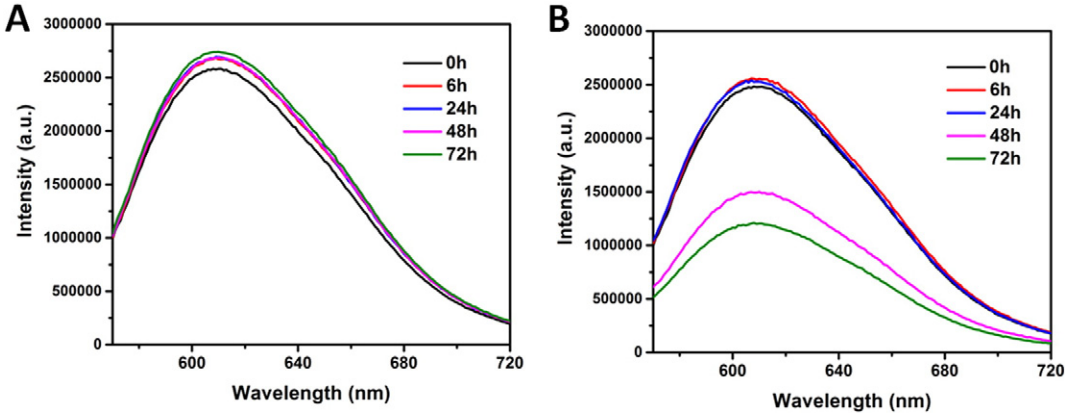

Figure 3. Changes in fluorescent intensity of Nile red-incorporated NPs in (**A**) distilled water and (**B**) PBS containing 10% FBS at 37 °C.

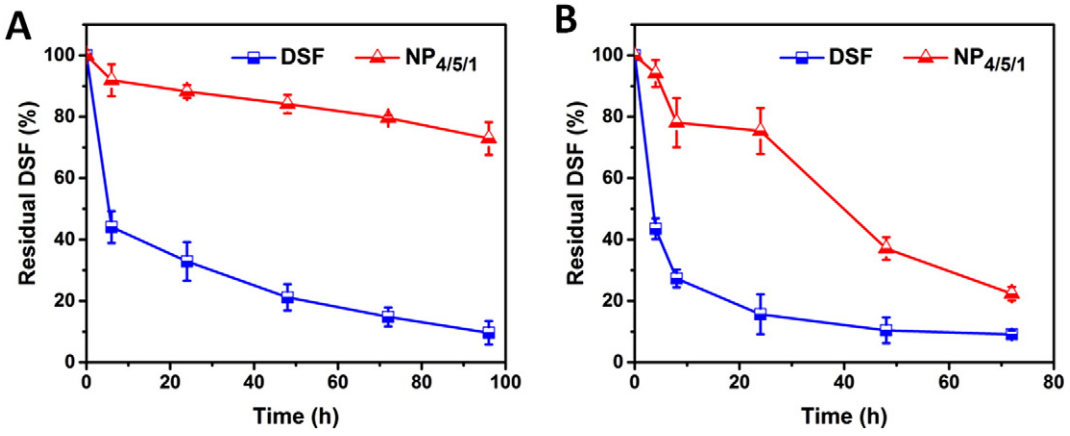

Figure 4. Residual DSF (%) of free DSF and $NP_{4/5/1}$ in (**A**) distilled water and (**B**) PBS containing 10% FBS at 37 °C (n = 3).

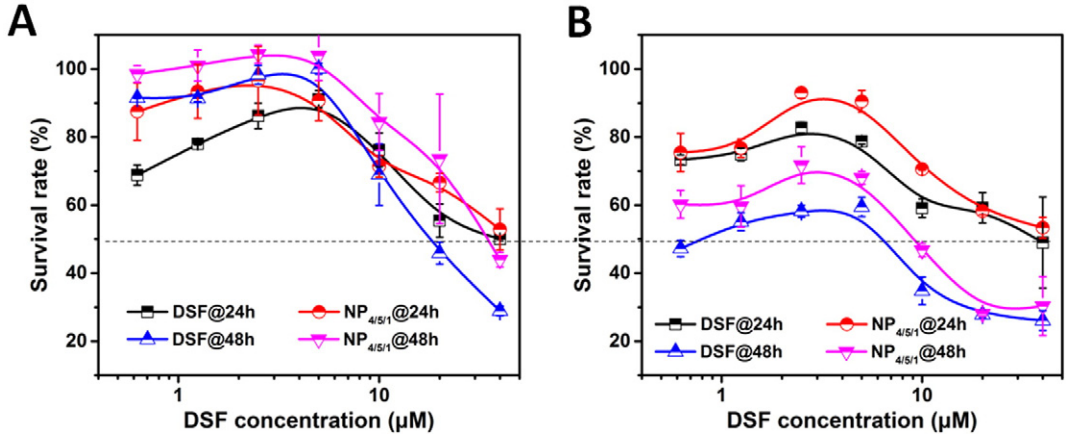

Figure 5. Cytotoxicity of DSF and $NP_{4/5/1}$ in (**A**) MCF-7 cells and (**B**) 4T1 cells at 24 and 48 h (n = 3).

quickly degraded in water, with only 43% left after 6 h, and less than 10% left after 96 h. In contrast, DSF loaded inside prepared NPs showed a significant reduction of its hydrolysis in water. After 96 h, over 70% of the DSF still remained. Similarly, the DSF concentration in PBS containing 10% FBS quickly degraded (Figure 4, *B*), while the DSF secured within the NPs maintained over 70% in 24 h. However, after 24 h, obvious DSF degradation occurred even with mPEG-PLGA/PCL NP encapsulation.

The above results showed that $NP_{4/5/1}$ remains quite stable in distilled water. Similarly, under near-physiological conditions (PBS containing 10% FBS), the $NP_{4/5/1}$ remained stable within a 24 h time period although the stability was decreased compared

Table 2
IC_{50} values of DSF and $NP_{4/5/1}$ in MCF-7 and 4T1 cells at 24 and 48 h.

		DSF/μM	$NP_{4/5/1}$/μM
MCF-7 cells	@24 h	40.0	>40.0
	@48 h	18.0	34.9
4T1 cells	@24 h	37.3	>40.0
	@48 h	6.3	9.1

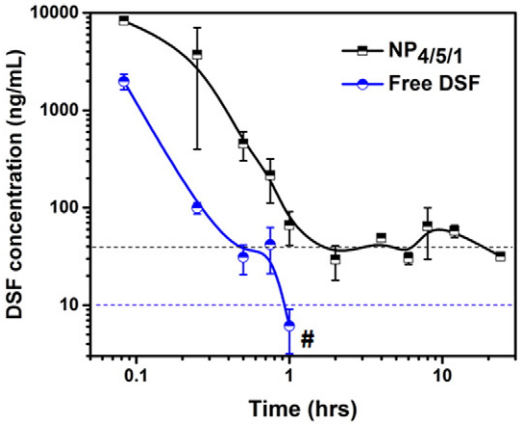

Figure 6. Time profiles of DSF concentration in plasma after i.v. administration of free DSF and $NP_{4/5/1}$ at a DSF dosage of 8.0 mg/kg. #, DSF could not be detected in the DSF group after 1 h. Each group is expressed as mean ± SD (n = 3).

to distilled water only. Based on these results, we conducted *in vitro* and *in vivo* tumor therapy tests.

In vitro cytotoxicity

The cytotoxicity of DSF and $NP_{4/5/1}$ to human breast cancer MCF-7 cells and murine breast cancer 4T1 cells was evaluated using the MTT assay. As shown in Figure 5, both free DSF and $NP_{4/5/1}$ inhibited tumor cell proliferation in a concentration-dependent manner. The IC_{50} values of $NP_{4/5/1}$ were higher than that of free DSF (Table 2), which may be partially attributed to the retarded release of DSF from the NPs. At 48 h, the IC_{50} values of free DSF and $NP_{4/5/1}$ in MCF-7 cells were 18.0 μM and 34.9 μM, respectively. In 4T1 cells, both free DSF and $NP_{4/5/1}$ had a stronger inhibitory effect compared with MCF-7 cells, with IC_{50} values of 6.3 μM for free DSF and 9.1 μM for $NP_{4/5/1}$ at 48 h.

We used Annexin-V-FITC and propidium iodide staining followed by FACS analysis in order to measure apoptosis in 4T1 cells treated with 1.0 μM free DSF or $NP_{4/5/1}$. As shown in Figure S1, $NP_{4/5/1}$ showed similar apoptotic effects compared with free DSF. We also measured the cellular uptake of the NPs in 4T1 cells by incubating them with NPs-Nile red. The NPs entered the tumor cells gradually after 1, 3 and 6 h (Figure S2). These results show that $NP_{4/5/1}$ is endocytosed by tumor cells, resulting in inhibition of the tumor cell growth and induction of apoptosis, suggesting significant potential in future tumor therapy studies.

Surface protein absorption in plasma

Prior to conducting *in vivo* studies, we tested the surface protein absorption properties of the $NP_{4/5/1}$ in plasma as reported by Docter et al.[46] As shown in Figure S3, no obvious protein absorption was observed on the $NP_{4/5/1}$ in 24 h of incubation with plasma, indicating the PEG shell effectively protected the NPs from interacting with the surrounding plasma proteins. We also tested the hydrodynamic radii of the NPs separated from the plasma after different incubation times; no obvious changes in size occurred during the observation period.

Table 3
Pharmacokinetic parameters of free DSF and $NP_{4/5/1}$.

Parameter	Free DSF	$NP_{4/5/1}$	Unit
AUC(0-∞)	452.3 ± 113.3	6108.0 ± 3352.4	mg/L * h
MRT(0-∞)	0.126 ± 0.042	8.74 ± 0.23	h
T_{max}	0.083	0.083	h
C_{max}	1984.7 ± 359.0	8310.6 ± 1575.2	mg/L
$T_{1/2}z$	0.165 ± 0.039	9.67 ± 0.21	h

AUC, area under curve; MRT, mean residence time; T_{max}, time to reach maximum concentration; C_{max}, maximum concentration; $T_{1/2}z$, terminal half life.

Pharmacokinetics

We compared the pharmacokinetics between free DSF and $NP_{4/5/1}$. Free DSF and $NP_{4/5/1}$ were administered via tail vein at a dosage of 8.0 mg/kg; blood samples were collected and analyzed immediately at 5 min, 15 min, 30 min, 45 min, 1 h, 2 h, 4 h, 6 h, 8 h, 12 h and 24 h after injection. As shown in Figure 6, free DSF quickly disappeared in blood after injection, with less than 10 ng/mL remaining at 1 h, and no detectable amount after 1 h. $NP_{4/5/1}$ significantly prolonged the blood retention time of DSF. Although the initial distribution was also quick, the DSF concentration was maintained around 40 ng/mL in blood for over 24 h. The pharmacokinetic parameters are summarized in Table 3. The T_{max} and C_{max} of both DSF and $NP_{4/5/1}$ appeared at the first time point (0.083 h); however, $NP_{4/5/1}$ significantly increased the AUC (6108.0 vs. 452.3 mg/L * h) and prolonged the MRT (8.74 vs. 0.126) and $T_{1/2}z$ (9.67 vs. 0.165). These data suggest that $NP_{4/5/1}$ enhanced the stability and availability of DSF *in vivo*, which addresses a key barrier against the *in vivo* delivery of DSF.

In vivo tumor therapy test

We used a 4T1 xenograft tumor model to test the efficacy of $NP_{4/5/1}$ as an anti-tumor therapeutic agent *in vivo*. Saline, DSF and $NP_{4/5/1}$ were administered on days 1, 3, 5, 8, 10 and 12 at a DSF dosage of 15.0 mg/kg. Tumor volumes and body weight changes were recorded. As shown in Figure 7, free DSF administered *via* tail vein showed almost no therapeutic effect, while $NP_{4/5/1}$ obviously slowed down the tumor growth rate. On day 24, the TSR % of $NP_{4/5/1}$ was 43.2%. Additionally, no obvious bodyweight loss was observed following administration of both formulas, demonstrating the safety of DSF and the $NP_{4/5/1}$. H&E staining of the tumor sections on day 24 also showed differences between the three groups. For saline and free DSF treatment, no obvious necrosis happened in the tumor tissues, while obvious necrosis regions could be seen in the $NP_{4/5/1}$ treated tumor tissues. The tumor therapy results support the hypothesis that $NP_{4/5/1}$ provides an adequate delivery system for DSF and

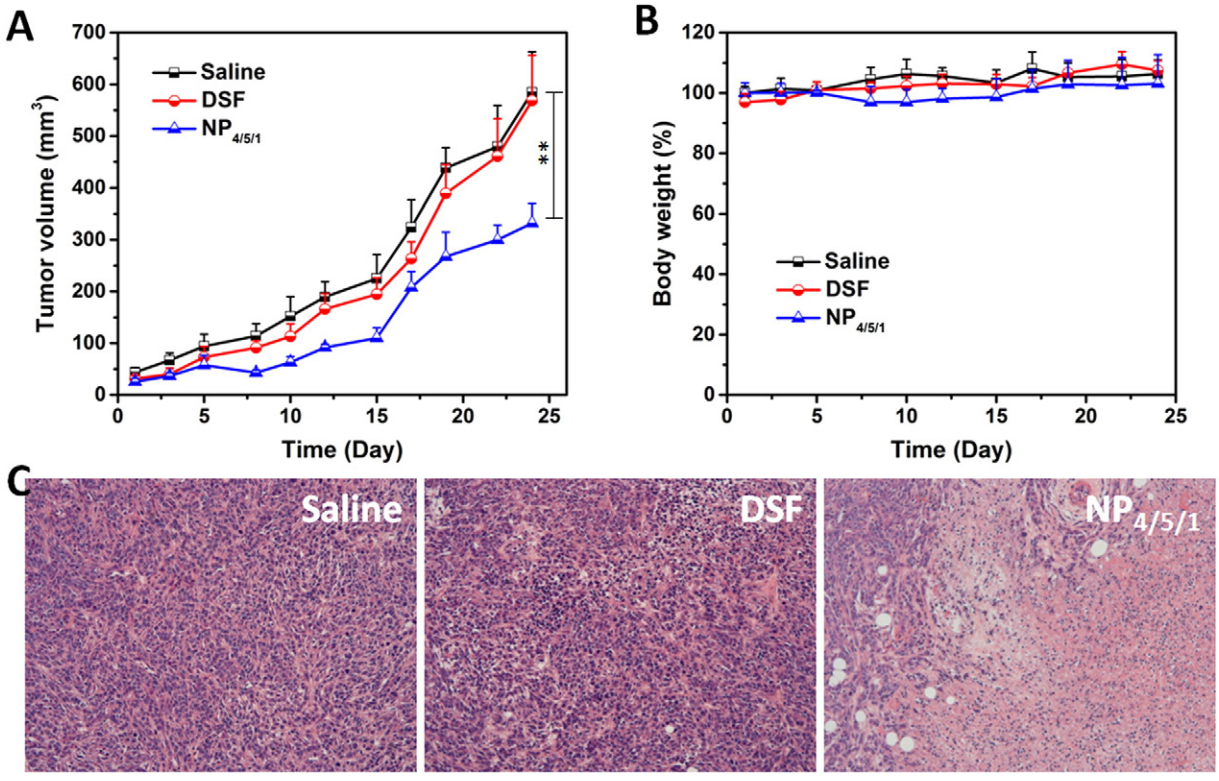

Figure 7. Tumor therapy test of DSF and $NP_{4/5/1}$ in a 4T1 xenograft tumor model. Drugs were administered on days 1, 3, 5, 8, 10, 12 at a DSF dosage of 15.0 mg/kg. Panels (**A**) and (**B**) are the recorded tumor volume and body weight changes, respectively. (**C**) Representative images of the tumor sections on day 24 using H&E staining. The images were taken at 4x magnitude. $^{**}P < 0.01$, $n = 6$.

protects against its premature degradation *in vivo* — providing an effective *in vivo* tumor therapy application.

Discussion

It has long been known that DSF has therapeutic potential for inhibition of tumor cell growth under *in vitro* conditions; however, this characteristic has not resulted in an effective treatment option *in vivo* due to extreme instability in a physiological environment. Obviously, a key issue for the successful application of DSF for cancer therapy is the design of a proper delivery system. Although a few studies have demonstrated that DSF can be encapsulated into liposomes or NPs, the encapsulation efficiency and loading stability have not been satisfactory, which has limited its therapeutic application.

In this study, we developed a simple and effective NP system for DSF loading and delivery. Since DSF undergoes self-catalyzed hydrolysis when coming into contact with water, we hypothesized that an NP system would be more suitable than liposomes for DSF loading. We then addressed two key issues associated with NPs-based delivery systems: the drug loading capability and drug loading stability. Commonly, the inclusion of higher hydrophobic segment contents results in an increased drug loading capability, while higher thermodynamic stability prevents drug leakage during the delivery process. Therefore, amphiphilic polymers with both hydrophilic and hydrophobic segments are necessary to prepare core-shell structure nanocarriers for drug entrapment.[47,48] Based on these analyses, we used $mPEG_{5k}$-$PLGA_{2k}$, a widely used polyester in biomedical application, as the matrix material in these studies.[49–51] Furthermore, the use of PCL is necessary for DSF encapsulation[30]; however, since high molecular weight PCL degrades slowly, PCL with a molecular weight of 3.4 k was applied here. The PCL content was adjusted by mixing different ratios of mPEG-PLGA and PCL.[52,53]

We applied a mixed system of mPEG-PLGA and PCL using the nanoprecipitation method shown in Scheme 1 and demonstrated that DSF could be immobilized in the formed NPs with a high, PCL concentration-dependent encapsulation efficiency (Figure 1, Table 1). In addition to increasing the encapsulation efficiency, an increasing PCL content increases the thermodynamic stability of the NPs. High thermodynamic stability is essential to keep the NPs and the cargo stably enwrapped inside. We confirmed this using the particle size and cargo-loading stability tests. The optimized $NP_{4/5/1}$ is stable in distilled water (Figure 2), and no cargo-release occurred for over 72 h as indicated by the Nile red intensity changes (Figure 3, *A*). Furthermore, the prepared $NP_{4/5/1}$ prevented the enwrapped DSF from degrading and maintained over 70% of the DSF residue in water within 96 h (Figure 4, *A*). Under near-physiological conditions (PBS containing 10% FBS), the stability of the NPs and the enwrapped cargos were gradually affected over time; obvious cargo loss or degradation was observed after 24 h (Figure 3, *B* and Figure 4, *B*). Protection of loaded cargos by the NPs occurs by separating the cargos from contact

with the outside medium. The results here reflect that the cargo-loading stability is not only governed by thermodynamic stability, but also kinetic principles.[35,37] Over time, substance diffusion inevitably occurs between the inside and outside of the NPs. Particularly in the near-physiological medium, cargo diffusion or degradation took place after 24 h. Nevertheless, the NPs substantially improved the cargo protection capacity within the first 24 h, which is a significant improvement for *in vivo* delivery as compared with the free DSF formulation.

Once we ensured that the $NP_{4/5/1}$ was optimally stable, we used MCF-7 and 4T1 cells to determine if the DSF maintained its tumor growth inhibitory properties (Figure 5). The $NP_{4/5/1}$ showed a tumor cell inhibition and apoptosis induction effect, although the IC_{50} values were higher than that of free DSF due to the retarded release of the drug from the NPs (Figure S1, Table 2). As mentioned above, the NPs slowly release DSF; therefore, we speculated that endocytosis is a major pathway for the loaded DSF to enter the tumor cells. We used CLSM to test this idea, as shown in Figure S2.

A pharmacokinetics study was used to provide more direct evidence for the effects of NPs-encapsulation and *in vivo* delivery of DSF. Historically, the key problem for *in vivo* administration of DSF is its quick degradation, resulting in little or no therapeutic amount of drug being delivered to the tumor tissue. We observed a significant difference in the plasma DSF concentration between free DSF and $NP_{4/5/1}$, however, a fast decrease also happened in the $NP_{4/5/1}$ group (Figure 6). *In vitro* plasma absorption tests showed that the mPEG shell can efficiently protect the NPs from protein absorption, and the size of the NPs kept constant over 24 h in plasma (Figure S3). In addition, the size of the NPs (R_h = 79.0 ± 9.3 nm) is within the proper range (20-200 nm) for avoiding premature elimination via glomerular filtration or the reticuloendothelial system (RES).[54] However, the *in vivo* situation is far more complicated than we can mimic, with additional factors such as fast shear flow and protein interactions. This may increase the contact possibility of the plasma medium with the loaded DSF and contribute to the fast DSF elimination of $NP_{4/5/1}$. Overall, the use of NPs as a drug carried increased the AUC of DSF 13.5 fold. The benefit from this was reflected in the tumor therapy results: free DSF showed almost no effect in tumor growth inhibition, while NP4/5/1 inhibited 43.2% of the tumor growth in 24 days (Figure 7).

In summary, we designed a robust delivery system for DSF that will increase the therapeutic applicability of DSF as an anti-tumor agent. Furthermore, these results may prove useful in the delivery of many other drugs that are unstable, or difficult to use in their original formula. A proper delivery system design may help these drugs be more meaningful for in vivo application.

Appendix A. Supplementary data

Supplementary data to this article can be found online at http://dx.doi.org/10.1016/j.nano.2015.10.022.

References

1. Chong CR, Sullivan DJ. New uses for old drugs. *Nature* 2007;**448**:645-6.
2. Ekins S, Williams AJ. Finding promiscuous old drugs for new uses. *Pharm Res Dordr* 2011;**28**:1785-91.
3. Kast RE, Boockvar JA, Bruning A, Cappello F, Chang WW, Cvek B, et al. A conceptually new treatment approach for relapsed glioblastoma: coordinated undermining of survival paths with nine repurposed drugs (CUSP9) by the International Initiative for Accelerated Improvement of Glioblastoma Care. *Oncotarget* 2013;**4**:502-30.
4. Azrin NH, Sisson RW, Meyers R, Godley M. Alcoholism treatment by disulfiram and community reinforcement therapy. *J Behav Ther Exp Psychiatry* 1982;**13**:105-12.
5. Conticello C, Martinetti D, Adamo L, Buccheri S, Giuffrida R, Parrinello N, et al. Disulfiram, an old drug with new potential therapeutic uses for human hematological malignancies. *Int J Cancer* 2012;**131**:2197-203.
6. Chen D, Cui QC, Yang H, Dou QP. Disulfiram, a clinically used anti-alcoholism drug and copper-binding agent, induces apoptotic cell death in breast cancer cultures and xenografts via inhibition of the proteasome activity. *Cancer Res* 2006;**66**:10425-33.
7. Cvek B, Dvorak Z. The value of proteasome inhibition in cancer. *Drug Discov Today* 2008;**13**:716-22.
8. Wickstrom M, Danielsson K, Rickardson L, Gullbo J, Nygren P, Isaksson A, et al. Pharmacological profiling of disulfiram using human tumor cell lines and human tumor cells from patients. *Biochem Pharmacol* 2007;**73**:25-33.
9. Yip NC, Fombon IS, Liu P, Brown S, Kannappan V, Armesilla AL, et al. Disulfiram modulated ROS-MAPK and NF kappa B pathways and targeted breast cancer cells with cancer stem cell-like properties. *Br J Cancer* 2011;**104**:1564-74.
10. Liu P, Kumar IS, Brown S, Kannappan V, Tawari PE, Tang JZ, et al. Disulfiram targets cancer stem-like cells and reverses resistance and cross-resistance in acquired paclitaxel-resistant triple-negative breast cancer cells. *Br J Cancer* 2013;**109**:1876-85.
11. Robinson TJW, Pai M, Liu JC, Vizeacoumar F, Sun T, Egan SE, et al. High-throughput screen identifies disulfiram as a potential therapeutic for triple-negative breast cancer cells Interaction with IQ motif-containing factors. *Cell Cycle* 2013;**12**:3013-24.
12. Hothi P, Martins TJ, Chen L, Deleyrolle L, Yoon JG, Reynolds B, et al. High-throughput chemical screens identify disulfiram as an inhibitor of human glioblastoma stem cells. *Oncotarget* 2012;**3**:1124-36.
13. Loo TW, Clarke DM. Blockage of drug resistance in vitro by disulfiram, a drug used to treat alcoholism. *J Natl Cancer Inst* 2000;**92**:898-902.
14. Loo TW, Bartlett MC, Clarke DM. Disulfiram metabolites permanently inactivate the human multidrug resistance P-glycoprotein. *Mol Pharm* 2004;**1**:426-33.
15. Brar SS, Grigg C, Wilson KS, Holder WD, Dreau D, Austin C, et al. Disulfiram inhibits activating transcription factor/cyclic AMP-responsive element binding protein and human melanoma growth in a metal-dependent manner in vitro, in mice and in a patient with metastatic disease. *Mol Cancer Ther* 2004;**3**:1049-60.
16. Zha J, Chen F, Dong H, Shi P, Yao Y, Zhang Y, et al. Disulfiram targeting lymphoid malignant cell lines via ROS-JNK activation as well as Nrf2 and NF-kappa B pathway inhibition. *J Transl Med* 2014;**12**:163.
17. Johansson B. Stabilization and quantitative-determination of disulfiram in human-plasma samples. *Clin Chim Acta* 1988;**177**:55-63.
18. Johansson B. A review of the pharmacokinetics and pharmacodynamics of disulfiram and its metabolites. *Acta Psychiatr Scand Suppl* 1992;**369**:15-26.
19. Peer D, Karp JM, Hong S, FaroKHzad OC, Margalit R, Langer R. Nanocarriers as an emerging platform for cancer therapy. *Nat Nanotechnol* 2007;**2**:751-60.
20. Yang XZ, Dou S, Sun TM, Mao CQ, Wang HX, Wang J. Systemic delivery of siRNA with cationic lipid assisted PEG-PLA nanoparticles for cancer therapy. *J Control Release* 2011;**156**:203-11.
21. Yang XZ, Dou S, Wang YC, Long HY, Xiong MH, Mao CQ, et al. Single-step assembly of cationic lipid-polymer hybrid nanoparticles for systemic delivery of siRNA. *ACS Nano* 2012;**6**:4955-65.

22. Song W, Tang Z, Li M, Lv S, Sun H, Deng M, et al. Polypeptide-based combination of paclitaxel and cisplatin for enhanced chemotherapy efficacy and reduced side-effects. *Acta Biomater* 2014;**10**:1392-402.
23. Li M, Tang Z, Lv S, Song W, Hong H, Jing X, et al. Cisplatin crosslinked pH-sensitive nanoparticles for efficient delivery. of doxorubicin. *Biomaterials* 2014;**35**:3851-64.
24. Lv S, Tang Z, Zhang D, Song W, Li M, Lin J, et al. Well-defined polymer-drug conjugate engineered with redox and pH-sensitive release mechanism for efficient delivery of paclitaxel. *J Control Release* 2014;**194**:220-7.
25. Yang T, Wang Y, Li Z, Dai W, Yin J, Liang L, et al. Targeted delivery of a combination therapy consisting of combretastatin A4 and low-dose doxorubicin against tumor neovasculature. *Nanomedicine* 2012;**8**:81-92.
26. Shen YQ, Zhou ZX, Sui MH, Tang JB, Xu PS, Van Kirk EA, et al. Charge-reversal polyamidoamine dendrimer for cascade nuclear drug delivery. *Nanomedicine* 2010;**5**:1205-17.
27. Parveen S, Misra R, Sahoo SK. Nanoparticles: a boon to drug delivery, therapeutics, diagnostics and imaging. *Nanomedicine* 2012;**8**:147-66.
28. Liu P, Wang Z, Brown S, Kannappan V, Tawari PE, Jiang W, et al. Liposome encapsulated Disulfiram inhibits NF kappa B pathway and targets breast cancer stem cells in vitro and in vivo. *Oncotarget* 2014;**5**:7471-85.
29. Duan X, Xiao J, Yin Q, Zhang Z, Yu H, Mao S, et al. Smart pH-sensitive and temporal-controlled polymeric micelles for effective combination therapy of doxorubicin and disulfiram. *ACS Nano* 2013;**7**:5858-69.
30. Loebler M, Rohm HW, Schmitz KP, Johnston AH, Newman TA, Ranjan S, et al. Drug delivery by nanoparticles — facing the obstacles. In: VanderSloten J, Verdonck P, Nyssen M, Haueisen J, editors. *4th European Conference of the International Federation for Medical and Biological Engineering*, 22; 2009. p. 2335-8.
31. Chen X, Zhang L, Hu X, Lin X, Zhang Y, Tang X. Formulation and preparation of a stable intravenous disulfiram-loaded lipid emulsion. *Eur J Lipid Sci Technol* 2015;**117**:869-78.
32. Hoda M, Sufi SA, Shakya G, Kumar KM, Rajagopalan R. Influence of stabilizers on the production of disulfiram-loaded poly(lactic-co-glycolic acid) nanoparticles and their anticancer potential. *Ther deliv* 2015;**6**:17-25.
33. Zembko I, Ahmed I, Farooq A, Dail J, Tawari P, Wang W, et al. Development of disulfiram-loaded poly(lactic-co-glycolic acid) wafers for the localised treatment of glioblastoma multiforme: a comparison of manufacturing techniques. *J Pharm Sci* 2015;**104**:1076-86.
34. Duan X, Xiao J, Yin Q, Zhang Z, Yu H, Mao S, et al. Multi-targeted inhibition of tumor growth and lung metastasis by redox-sensitive shell crosslinked micelles loading disulfiram. *Nanotechnology* 2014;**25**:125102.
35. Sun Q, Radosz M, Shen Y. Challenges in design of translational nanocarriers. *J Control Release* 2012;**164**:156-69.
36. Kwon GS. Polymeric micelles for delivery of poorly water-soluble compounds. *Crit Rev Ther Drug Carrier Syst* 2003;**20**:357-403.
37. Ke X, Ng VWL, Ono RJ, Chan JMW, Krishnamurthy S, Wang Y, et al. Role of non-covalent and covalent interactions in cargo loading capacity and stability of polymeric micelles. *J Control Release* 2014;**193**:9-26.
38. Lu Y, Park K. Polymeric micelles and alternative nanonized delivery vehicles for poorly soluble drugs. *Int J Pharm* 2013;**453**:198-214.
39. Kim S, Shi Y, Kim JY, Park K, Cheng JX. Overcoming the barriers in micellar drug delivery: loading efficiency, in vivo stability, and micelle-cell interaction. *Expert Opin Drug Deliv* 2010;**7**:49-62.
40. Attia ABE, Ong ZY, Hedrick JL, Lee PP, Ee PLR, Hammond PT, et al. Mixed micelles self-assembled from block copolymers for drug delivery. *Curr Opin Colloid Interface Sci* 2011;**16**:182-94.
41. Song W, Tang Z, Zhang D, Zhang Y, Yu H, Li M, et al. Anti-tumor efficacy of c(RGDfK)-decorated polypeptide-based micelles co-loaded with docetaxel and cisplatin. *Biomaterials* 2014;**35**:3005-14.
42. Yu H, Tang Z, Zhang D, Song W, Zhang Y, Yang Y, et al. Pharmacokinetics, biodistribution and in vivo efficacy of cisplatin loaded poly(L-glutamic acid)-*g*-methoxy poly(ethylene glycol) complex nanoparticles for tumor therapy. *J Control Release* 2015;**205**:89-97.
43. Song W, Tang Z, Li M, Lv S, Yu H, Ma L, et al. Tunable pH-sensitive poly(beta-amino ester)s synthesized from primary amines and diacrylates for intracellular drug delivery. *Macromol Biosci* 2012;**12**:1375-83.
44. Lewis DJ, Deshmukh P, Tedstone AA, Tuna F, O'Brien P. On the interaction of copper(II) with disulfiram. *Chem Commun* 2014;**50**:13334-7.
45. Cen DZ, Brayton D, Shahandeh B, Meyskens FL, Farmer PJ. Disulfiram facilitates intracellular Cu uptake and induces apoptosis in human melanoma cells. *J Med Chem* 2004;**47**:6914-20.
46. Docter D, Distler U, Storck W, Kuharev J, Wunsch D, Hahlbrock A, et al. Quantitative profiling of the protein coronas that form around nanoparticles. *Nat Protoc* 2014;**9**:2030-44.
47. Nishiyama N, Kataoka K. Current state, achievements, and future prospects of polymeric micelles as nanocarriers for drug and gene delivery. *Pharmacol Ther* 2006;**112**:630-48.
48. Adams ML, Lavasanifar A, Kwon GS. Amphiphilic block copolymers for drug delivery. *J Pharm Sci* 2003;**92**:1343-55.
49. He Z, Sun Y, Wang Q, Shen M, Zhu M, Li F, et al. Degradation and biosafety evaluation of mPEG-PLGA-PLL copolymer-prepared nanoparticles. *J Phys Chem C* 2015;**119**:3348-62.
50. Wang Y, Liu P, Duan Y, Yin X, Wang Q, Liu X, et al. Specific cell targeting with APRPG conjugated PEG-PLGA nanoparticles for treating ovarian cancer. *Biomaterials* 2014;**35**:983-92.
51. Okada H, Toguchi H. Biodegradable microspheres in drug-delivery. *Crit Rev Ther Drug Carrier Syst* 1995;**12**:1-99.
52. Sun HF, Mei L, Song CX, Cui XM, Wang PY. The in vivo degradation, absorption and excretion of PCL-based implant. *Biomaterials* 2006;**27**:1735-40.
53. Shen YQ, Sun WL, Zhu KJ, Shen ZQ. Regulation of biodegradability and drug release behavior of aliphatic polyesters by blending. *J Biomed Mater Res* 2000;**50**:528-35.
54. Maeda H, Nakamura H, Fang J. The EPR effect for macromolecular drug delivery to solid tumors: Improvement of tumor uptake, lowering of systemic toxicity, and distinct tumor imaging in vivo. *Adv Drug Deliv Rev* 2000;**50**:528-35.